

# Composite Dipolar Recoupling: Anisotropy Compensated Coherence Transfer in Solid-State NMR

Navin Khaneja\*, Cindie Kehlet<sup>†</sup>, Steffen J. Glaser<sup>‡</sup>, Niels Chr. Nielsen<sup>§</sup>

August 30, 2018

## Abstract

The efficiency of dipole-dipole coupling driven coherence transfer experiments in solid-state NMR spectroscopy of powder samples is limited by dispersion of the orientation of the internuclear vectors relative to the external magnetic field. Here we introduce general design principles and resulting pulse sequences that approach full polarization transfer efficiency for all crystallite orientations in a powder in magic-angle-spinning experiments. The methods compensate for the defocusing of coherence due to orientation dependent dipolar coupling interactions and inhomogeneous radio-frequency fields. The compensation scheme is very simple to implement as a scaffold (comb) of compensating pulses in which the pulse sequence to be improved may be inserted. The degree of compensation can be adjusted and should be balanced as a compromise between efficiency and length of the overall pulse sequence. We show by numerical and experimental data that the presented compensation protocol significantly improves the efficiency of known dipolar recoupling solid-state NMR experiment.

\*Corresponding author: Email:navin@hrl.harvard.edu. Division of Engineering and Applied Sciences, Harvard University, Cambridge, MA 02138. The work was supported by ONR 38A-1077404, AFOSR FA9550-05-1-0443 and AFOSR FA9550-04-1-0427

<sup>†</sup>Centre for Insoluble Protein Structures (inSPIN), Interdisciplinary Nanoscience Center (iNANO) and Department of Chemistry, University of Aarhus, Denmark

<sup>‡</sup>Department of Chemistry, Technische Universität München, 85747 Garching, Germany. This work was supported by the Deutsche Forschungsgemeinschaft, grant GI 203/4-2.

<sup>§</sup>Corresponding author: Email: ncn@chem.au.dk. Centre for Insoluble Protein Structures (inSPIN), Interdisciplinary Nanoscience Center (iNANO) and Department of Chemistry, University of Aarhus, Denmark. The work was supported by the Danish National Research Foundation, Carlsbergfondet, The Danish Natural Science Research Council, and the Danish Biotechnological Instrumentcentre (DABIC).

# 1 Introduction

Nuclear magnetic resonance (NMR) spectroscopy is rapidly finding increasingly important applications for atomic-resolution structural analysis of biological macromolecules in the solid phase [1, 2, 3, 4, 5]. This opens up new avenues for studying "insoluble" protein structures such as membrane proteins, fibrils, and extracellular matrix proteins which are exceedingly difficult to analyze using conventional atomic-resolution structure determination methods, including liquid-state NMR and X-ray crystallography. The progress in biological solid-state NMR relies on continuous development of instrumentation, sample preparation methods, and the underlying NMR methodology. The goal of studying increasingly complex molecular systems is a strong motivation for the development of improved solid-state NMR methods.

The latter challenge motivates the present paper, where we address a fundamental problem of coherence transfer in solid-state NMR of "powder" samples. For solids, the internal Hamiltonian not only contains isotropic interactions, such as isotropic chemical shifts and scalar  $J$  couplings, but also anisotropic (i.e., orientation dependent) chemical shifts and dipole-dipole coupling interactions in the case of coupled spin-1/2 nuclei. This implies that each molecule/crystallite in a "powder" sample may exhibit different nuclear spin interactions leading to severe line broadening and thereby reduced spectral resolution and sensitivity. This problem may be alleviated using magic-angle spinning (MAS), which averages these interactions and hereby results in high-resolution conditions for solid samples. However, this also results in loss of useful parts of the anisotropic interactions like dipolar couplings, which carry information about distances between nuclei and can help in obtaining structural information. This has triggered the development of dipolar recoupling techniques [6, 7, 8, 9, 10, 11, 12], which selectively reintroduce these couplings to enable measurement of internuclear distances, torsion angles, and transfer of magnetization from spin to spin in the molecule. Such recoupling experiments are the building blocks of essentially all biological solid-state NMR experiments using "powder" samples. However, the orientation dependence of the dipolar coupling interaction poses a fundamental challenge for the design of experiments, e.g. for transfer of coherence between spins using dipolar couplings, that are insensitive to the orientation dependence.

The orientation dependency of the dipolar coupling is characterized by Euler angles  $\beta$  and  $\gamma$  expressing the angle between the internuclear axis and the MAS rotor and the rotation of the crystallite around the rotor axis, respectively. The discovery of the so called  $\gamma$ -encoded dipolar recoupling by

Nielsen and coworkers [9] in 1994, showed that it is possible to eliminate the dependency of coherence transfer efficiency on the angle  $\gamma$  and increase the transfer efficiency to 73% from the previously accepted maximum of 50%. In this paper, we map the problem of dipolar recoupling in the presence of anisotropies in  $\beta$  and the strength of rf field to a problem of control of single spin in the presence of rf-inhomogeneity and Larmor dispersion. Using this analogy, we demonstrate how relatively simple procedures can combine the concepts of solid-state NMR  $\gamma$ -encoded recoupling [2, 7, 8, 9, 10, 11, 12], based on coherent averaging methods [13, 14, 15], with the concepts of composite pulse sequences [16, 17, 18] from liquid-state NMR to make experiments insensitive to angle  $\beta$ . It is now possible to construct a family of dipolar recoupling experiments of increasing length and degree of compensation that ultimately achieve 100% transfer efficiency for all orientations of the dipolar coupling tensor. In practice, the desired level of compensation needs to be traded against increased loss of signal due to relaxation during the increased pulse sequence duration. We show that besides being less sensitive to the orientational dependencies, the compensated recoupling experiments are also more robust towards resonance offsets and instrumental artifacts like rf inhomogeneity. The general design principle is demonstrated by applications to heteronuclear dipolar recoupling and similar applications for homonuclear dipolar recoupling are described. Using these compensated pulse sequences, we provide experimental performances similar to those obtained using optimal control procedures [19, 20] and recently demonstrated in solid-state NMR [21, 22].

## 2 Theory

Consider two coupled heteronuclear spins  $I$  and  $S$  under magic angle spinning. The spins are irradiated with rf fields at their Larmor frequencies along say the  $x$  direction. In a doubly rotating Zeeman frame, rotating with both the spins at their Larmor frequency, the Hamiltonian of the system takes the form

$$H(t) = \omega_I(t)I_z + \omega_S(t)S_z + \omega_{IS}(t)2I_zS_z + \omega_{rf}^I(t)I_x + \omega_{rf}^S(t)S_x \quad , \quad (1)$$

where  $\omega_I(t)$ ,  $\omega_S(t)$ , and  $\omega_{IS}(t)$  represent time-varying chemical shifts for the two spins  $I$  and  $S$  and the coupling between them, respectively. These interactions may be expressed as Fourier series  $\omega_\lambda(t) = \sum_{m=-2}^2 \omega_\lambda^m \exp(im\omega_r t)$ , where  $\omega_r$  is the spinning frequency (in angular units), while the coefficients  $\omega_\lambda$  ( $\lambda = I, S, IS$ ) reflect the dependence on the physical parameters like the isotropic chemical shift, anisotropic chemical shift, the dipole-dipole coupling constant and through this the internuclear distance [23].  $\omega_{rf}^I(t)$  and  $\omega_{rf}^S(t)$  are amplitudes of the rf fields on spins  $I$  and  $S$ ,

respectively. When the rf field strengths on the two spins is chosen to be integral (or half integral) multiples of spinning frequency, i.e.,  $\omega_{rf}^I = p\omega_r$  and  $\omega_{rf}^S = q\omega_r$ , the Hamiltonian for the dipole-dipole coupling in the interaction frame of the rf irradiation averages over a rotor period to [27, 28]

$$\bar{H}_{IS} = (A_{p+q}^+ Z^+ - iA_{p+q}^- Y^+) + (A_{p-q}^+ Z^- - iA_{p-q}^- Y^-) \quad , \quad (2)$$

where  $A_n^\pm = \frac{1}{2}(\omega_{IS}^{-(n)} \pm \omega_{IS}^{(n)})$ ,  $Z^\pm = I_z S_z \mp I_y S_y$  and  $Y^\pm = I_y S_z \pm I_z S_y$ . For convenience, we also define the operator  $X^\pm = \frac{1}{2}(I_x \pm S_x)$ , which completes the formation of two three-dimensional operator subspaces  $X^-$ ,  $Y^-$ ,  $Z^-$  and  $X^+$ ,  $Y^+$ ,  $Z^+$  (the two subspaces are respectively zero- and double-quantum operators in a frame tilted by  $\pi/2$  around the  $I_y$  and  $S_y$  axes).

Using this notation, the widely used Double Cross Polarization (DCP) [6] experiment may be described by choosing  $p - q = \pm 1$  and  $|p + q| > 2$  to obtain

$$\bar{H}_{IS}^{(\pm 1)} = \kappa[\cos(\gamma)Z^- \pm \sin(\gamma)Y^-] \quad , \quad (3)$$

where  $\gamma$  as before is the Euler angle discriminating the crystallites by rotations around the rotor axis. The scaling factor  $\kappa = \frac{1}{2\sqrt{2}}b_{IS}\sin(2\beta)$  depends on the dipole-dipole coupling constant  $b_{IS}$  and the angle  $\beta$  between the internuclear axis and the rotor axis. This effective Hamiltonian mediates the coherence transfer  $I_x \rightarrow S_x$  with an efficiency independent on the  $\gamma$  Euler angle. The details of the transfer process become transparent by decomposing  $I_x = X^+ + X^-$  and observing that the effective Hamiltonian  $\bar{H}_{IS}^{(\pm 1)}$ , commutes with the operator  $X^+$ , while the operator  $X^-$  undergoes the transformation

$$X^- \rightarrow \cos(\kappa t)X^- + \sin(\kappa t)[\cos(\gamma)Y^- \mp \sin(\gamma)Z^-] \quad , \quad (4)$$

where the maximum transfer onto  $S_x = X^+ - X^-$  is obtained when  $\cos(\kappa t) = -1$  [27, 28] (In the subsequent text  $\pm 1$  in  $\bar{H}_{IS}^{(\pm 1)}$  is omitted for simplicity).

If there is no dispersion in  $\kappa$ , evolution under the effective Hamiltonian in Eq. (3) in  $\frac{\pi}{\kappa}$  units of time leads to inversion of  $X^-$  and makes a complete  $I_x \rightarrow S_x$  transfer. For a powder sample, however, the dispersion in  $\kappa$  has the consequence that for no single evolution time complete polarization transfer for all orientations can be achieved. The evolution time is therefore chosen for a nominal value  $\kappa_0$  such that it gives the optimal polarization transfer of 73% when averaged over the whole powder [28]. For a powder sample this leads to trajectories of the type shown in Fig. 1a. The trajectories correspond to different values of  $\gamma$  and a specific  $\beta$  value that executes 86% of a full  $\pi$  rotation. The corresponding DCP pulse sequence is shown in Fig. 2a. It is clear from Fig. 1a

that while the paths of the various trajectories depend on the  $\gamma$  crystallite angle, the net transfer is independent of  $\gamma$ . It is also clear that, except for the ideal  $\kappa t = \pi$  rotation, there will be a loss in transfer efficiency.

It is possible to compensate for dispersion in the value of  $\beta$  (hence  $\kappa$ ) by composing the evolution of the spin system under  $\bar{H}_{IS}$  with supplementary rf rotations to achieve a compensating effect very similar to composite pulses in liquid-state NMR [18]. The basic idea of this compensation is illustrated in Fig. 1b by a trajectory starting with an initial operator  $X^-$  (the angle  $\gamma$  is chosen to be 0). The parts of the trajectory labeled *I*, *III*, and *V* denote the evolution under the effective Hamiltonian  $\bar{H}_{IS}$  for duration corresponding to nominal rotation angles  $\frac{\pi}{2}$ ,  $\pi$ , and  $\frac{\pi}{2}$ , respectively. The sections *II* and *IV* of the trajectory represent a  $-\frac{\pi}{2}$  and  $\frac{\pi}{2}$  angle rotation under the rf Hamiltonian  $X^-$ , respectively. A  $\frac{\pi}{2}$  rotation around  $X^-$  can be achieved by  $x$ -phase  $\frac{\pi}{2}$  pulse on the *I*- or the *S*-spin rf channel. Alternatively one may apply  $\frac{\pi}{4}$  pulses on both channels. The compensation in dispersion of  $\beta$  is immediate from the trajectory. The internuclear vectors with a larger value of  $\kappa$  execute a bigger rotation during the phase *I* of the trajectory. The compensating  $\pi$  rotation (phase *III*) swaps (approximately) the position of internuclear vectors with values  $\kappa_0(1 + \epsilon)$  and  $\kappa_0(1 - \epsilon)$ , where  $\epsilon$  is the fractional dispersion from the nominal value  $\kappa_0$ . In the final phase (phase *V*) the larger values  $\kappa_0(1 + \epsilon)$  catch up with  $\kappa_0(1 - \epsilon)$  at the end point. The corresponding unitary evolution is described by the propagator

$$U = \exp(-i\bar{H}_{IS}t_{\frac{\pi}{2}}) \exp(-i\frac{\pi}{2}X^-) \exp(-i\bar{H}_{IS}t_{\pi}) \exp(i\frac{\pi}{2}X^-) \exp(-i\bar{H}_{IS}t_{\frac{\pi}{2}}) \quad , \quad (5)$$

where  $t_{\frac{\pi}{2}}$  and  $t_{\pi}$  denote nominal evolution periods for  $\pi/2$  and  $\pi$  rotations under influence of  $\bar{H}_{IS}$ . The propagator can be experimentally realized using the pulse sequence in Fig. 2b. The sequence comprises three evolution periods of the DCP Hamiltonian  $\bar{H}_{IS}$  inserted into a scaffold (comb) of phase correcting pulses and will henceforth be referred to as COMB<sub>3</sub>DCP. The term COMB, proposed for future reference, stands for compensated for beta, which is a concept which adds efficiency as a complement to gamma encoding.

The compensated recoupling is in complete analogy with the classic  $(\pi/2)_y(\pi)_{\bar{x}}(\pi/2)_y$  inversion pulse that is commonly used to compensate for rf inhomogeneity in liquid-state NMR [16, 18]. In Fig. 1b, the  $(\pi/2)_y$  parts of the pulse sequence are the phases *I* and *V* of the trajectory and corresponds to the evolution of  $\bar{H}_{IS}$ . The  $(\pi)_{\bar{x}}$  rotation is achieved by the segments *II–III–IV* and corresponds to the unitary transformation  $\exp(-i\frac{\pi}{2}X^-) \exp(-i\bar{H}_{IS}t_{\pi}) \exp(i\frac{\pi}{2}X^-)$ . The  $\frac{\pi}{2}$  rotations around  $X^-$  take significantly less time compared to the evolution of  $\bar{H}_{IS}$ . The methodology presented here

works for all values of  $\gamma$ , merely leading to a rotation of the trajectory around the  $X^-$  axis, and therefore preserves the attractive  $\gamma$ -encoding property [9, 28] of the standard DCP experiment and in addition compensates for the dispersion in the  $\beta$  crystallite angle. The picture in Fig. 1b presents a simple one spin analogy between well studied composite rf pulses in liquid-state NMR with the conceptually more complex coherence transfers between coupled spins under MAS conditions. We note that similar analogy has been exploited before in liquid state NMR for e.g., in ‘‘RJCP’’ compensation schemes [24, 25] (see [26] for a review). This analogy immediately helps us to construct more elaborate anisotropy compensation schemes like dipolar-recoupling analogs to the composite pulse  $(3\pi/2)_{\bar{x}}(2\pi)_x(\pi/2)_y(3\pi/2)_{\bar{y}}(2\pi)_y(\pi/2)_x$  [17]. The various phases are obtained by simply observing that the phase of rotation under  $\bar{H}_{IS}$  can be advanced by  $\theta$  by inserting the evolution under  $\bar{H}_{IS}$  between a  $-\theta$  and  $\theta$  rotation around  $X^-$ . In shorthand notation the sequence may be written:  $3t_{\pi/2} - (\pi/2)_{\bar{x}}^I(\pi/2)_x^S - 4t_{\pi/2} - (\pi/4)_{\bar{x}}^I(\pi/4)_x^S - t_{\pi/2} - (\pi/2)_{\bar{x}}^I(\pi/2)_x^S - 3t_{\pi/2} - (\pi/2)_{\bar{x}}^I(\pi/2)_x^S - 4t_{\pi/2} - (\pi/4)_{\bar{x}}^I(\pi/4)_x^S - t_{\pi/2}$ , where  $t_{\pi/2}$  corresponds to a period with DCP-matched rf irradiation corresponding to a  $\pi/2$  rotation under action of  $\bar{H}_{IS}$ . This sequence will henceforth be referred to as COMB<sub>6</sub>DCP.

The role of rf inhomogeneity also becomes transparent in this single spin analogy to the two-spin coherence transfer process in Fig. 1b. If  $\Delta\omega_{rf}^I$  and  $\Delta\omega_{rf}^S$  represents the dispersion in the  $I$ - and  $S$ -spin rf field strengths from their nominal values then the effective Hamiltonian in Eq. (3) is modified to

$$\bar{H} = \bar{H}_{IS} + \Delta\omega_{rf}^- X^- + \Delta\omega_{rf}^+ X^+ \quad , \quad (6)$$

where  $\Delta\omega_{rf}^\pm = \frac{1}{2}(\Delta\omega_{rf}^I \pm \Delta\omega_{rf}^S)$ . The operator  $X^+$  commutes with  $\bar{H}_{IS}$  and consequently has no effect on evolution of the initial coherence  $I_x$ . In the single spin analogy, the term  $\Delta\omega_{rf}^- X^-$  produces an uncontrolled rotation around  $X^-$  axis and acts like a Larmor frequency (or resonance offset) dispersion in Fig. 1b. Therefore, the anisotropies in  $\beta$  and rf-field strengths translate to problems of rf-inhomogeneity and frequency dispersion in the single spin picture in Fig. 1. Compensating for both these dispersions in recoupling experiments is reduced to finding an inversion pulse that compensates both for rf inhomogeneity and resonance offset. The  $(\pi/2)_y(\pi)_{\bar{x}}(\pi/2)_y$  and  $(3\pi/2)_{\bar{x}}(2\pi)_x(\pi/2)_y(3\pi/2)_{\bar{y}}(2\pi)_y(\pi/2)_x$  pulse schemes do provide compensation for both these dispersions. It is possible now to construct more elaborate compensation schemes that achieve a higher level of compensation.

The increased level of compensation comes at the cost of a longer pulse sequence. This naturally

leads to the problem of finding the shortest possible pulse sequence that achieves a desired level of compensation for a prescribed distribution of the angle  $\beta$  and inhomogeneity in rf-field strength. This is a problem in optimal control [19] and can be addressed rigorously in this framework as done recently in a numerical approach [21]. The analogy of dipolar recoupling to control of single spin reduces the problem of designing short and robust recoupling experiments in the presence of dispersion in  $\beta$  and rf-field strength to design of short inversion pulses for a single spin that are robust to Larmor dispersion and rf-inhomogeneity. This problem has recently been studied in detail in the framework of optimal control [29]. It is expected that many of these ideas and techniques can be directly translated to design recoupling experiments that achieve compensation comparable to adiabatic sequences in a much shorter time [30, 31]. The single spin analogy also offers an explanation to the superior performance of numerical optimal control procedures demonstrated in solid state NMR recoupling experiments [21, 22].

The ideas presented above are not restricted to dipolar recoupling driven heteronuclear coherence transfer but may also readily be adapted to obtain anisotropy compensated homonuclear dipolar recoupling. This becomes evident if we consider two dipolar coupled homonuclear spins  $I$  and  $S$  for which the MAS modulated dipolar-coupling Hamiltonian is of the form

$$H_{IS}(t) = \omega_{IS}(t)(\mathbf{I}\cdot\mathbf{S} - 3I_zS_z) \quad (7)$$

In the interaction frame of a non-selective constant-phase rf irradiation, the  $\omega_{IS}(t)\mathbf{I}\cdot\mathbf{S}$  component averages to zero over a rotor period as the operator term  $\mathbf{I}\cdot\mathbf{S}$  commutes with the rf Hamiltonian (e.g.,  $I_x + S_x$ ). This leaves us with the modulation of the  $3I_zS_z$  component, and a formalism very similar to that described above for the heteronuclear case applies. The only difference is that one has non-selective rf irradiation in this case and as a result one manipulates operators of the type  $X^+$  instead of the differential operator  $X^-$ . A good example is the HORROR experiment [9] in which the two spins are irradiated at their mean resonance frequency by a rf field with the amplitude  $\omega_{rf}$  adjusted to half the rotor frequency, i.e.,  $\omega_{rf} = \frac{1}{2}\omega_r$ . Using Eq. (2) with  $p = q = \frac{1}{2}$  the dipolar coupling Hamiltonian in the interaction frame of the rf irradiation averages over a rotor period to

$$\bar{H}_{IS} = \kappa[\cos(\gamma)Z^+ + \sin(\gamma)Y^+], \quad (8)$$

with  $\kappa = \frac{3}{4\sqrt{2}}b_{IS}\sin(2\beta)$ . In this case the effective Hamiltonian commutes with the operator  $X^-$  and inverts  $X^+$  after a time evolution corresponding to a  $\pi$  pulse. This situation may be represented by the diagram in Fig. 1a except interchanging the "zero-quantum" coordinate system  $\{X^-, Y^-, Z^-\}$  with the corresponding "double-quantum" coordinate system  $\{X^+, Y^+, Z^+\}$ . Within this framework

we can compensate for dispersions in the dipolar coupling scaling factor  $\kappa$  using the same composite sequences as used for the DCP experiment, by replacing the rotations in segments II and IV of the trajectories (Fig. 1b) by  $\frac{\pi}{2}$  rotations produced by rf Hamiltonian  $X^+ = \frac{I_x + S_x}{2}$ . As described above, more elaborate compensation schemes that simultaneously compensate for the dispersion in  $\beta$  and inhomogeneity in rf field can also be found in this case.

Finally, it is relevant to mention that the COMB dipolar recoupling is not restricted to its analogy with liquid-state NMR composite  $\pi$  inversion pulses. Compensated  $\pi/2$  excitation pulses may serve as inspiration to design dipolar recoupling experiments for which it is relevant to excite coherences at the equator of the three-dimensional operator representations in Fig. 1. This may be the case, for example, in double- or zero-quantum experiments where, e.g. double-quantum filtration or coherence evolution may provide information about spin topologies or through coupling to other spins information about dihedral angles. One example could be the double-quantum (2Q) HORROR experiment [9] where  $\gamma$ -encoded excitation and reconversion of double-quantum coherences is an intrinsic element. In this case it is possible to maintain  $\gamma$ -encoding and compensate for dispersions in the dipolar coupling using composite excitation pulses such as the classic  $(\pi/2)_x(\pi)_{y+\pi/6}$  composite excitation pulse.

### 3 Results and Discussion

A first impression of the performance of the anisotropy compensated heteronuclear dipolar recoupling DCP experiments relative to the conventional DCP experiment is illustrated in Fig. 3a with numerical calculations of the efficiency of a typical  $^{15}\text{N} \rightarrow ^{13}\text{C}$  coherence transfer as function of the excitation period. The calculations address specifically the  $^{13}\text{C}_\alpha$ - $^{15}\text{N}$  spin pair of glycine in a powder sample subject to 10 kHz MAS, an external magnetic field corresponding to a 700 MHz (Larmor frequency for  $^1\text{H}$ ) spectrometer, and nominal rf field strengths on the  $^{13}\text{C}$  and  $^{15}\text{N}$  channels of 35 and 25 kHz, respectively. These graphs reveal that the compensated schemes indeed increases the efficiency of 70.2% for the  $\gamma$ -encoded DCP experiment to 80.9% and 87.1% for the three- and six-pulse compensated schemes under conditions of homogeneous rf fields (we note the theoretical numbers for the ideal case without chemical shielding anisotropies etc, and perfect digitization of the rotor period are slightly higher). This corresponds to gain factors of 1.15 and 1.24 for COMB<sub>3</sub>DCP and COMB<sub>6</sub>DCP, respectively. Under 2% Lorentzian rf inhomogeneity the corresponding gain factors increase to 1.21 and 1.29, while they increase to 1.38 and 1.83 for 5% Lorentzian rf inhomogeneity.

We note that in these evaluations the effect of 5% Lorentzian rf inhomogeneity resemble 9 - 10% Gaussian inhomogeneity both of which being representative for the inhomogeneity of typical 2.5 - 4 mm solid-state NMR rotors.

It is clear from the graphs in Fig. 3a that composite recoupling experiments not only improve the transfer efficiency in terms of compensation for dispersions in the dipolar coupling but also provides significant improvements by compensation of rf inhomogeneity effects. It is also clear that the length of the pulse sequences increases substantially for the establishment of the most efficient compensation and that a compromise has to be taken experimentally to avoid excessive loss due to relaxation. This aspect becomes clear in Fig. 3b showing experimental  $^{13}\text{C}$  spectra of glycine obtained using a triple resonance transfer scheme using CP for  $^1\text{H} \rightarrow ^{15}\text{N}$  transfer and DCP, COMB<sub>3</sub>DCP or COMB<sub>6</sub>DCP for  $^{15}\text{N} \rightarrow ^{13}\text{C}$  transfer (layout as in Fig. 2) using the same conditions as described for the numerical simulation. The experiments were acquired using a BRUKER AVANCE 700 MHz NMR spectrometer using a standard 2.5 mm triple-resonance MAS probe. The rf inhomogeneity of a full 2.5 mm MAS rotor resembles a 5% Lorentzian shape. The experimental spectra show a gain factor 1.34 for COMB<sub>3</sub>DCP relative to DCP, while no experimental gain was obtain using the somewhat longer COMB<sub>6</sub>DCP pulse sequence. This loss of gain can most likely be attributed to relaxation effects.

A clearer picture of the compensating effect of the composite recoupling experiments is given in Fig. 4 by 3D plots of the transfer efficiency as function of the rf inhomogeneity parameter  $\omega_{rf}/\omega_{rf}^{nom}$  and the dipolar coupling deviation parameter  $\omega_D/\omega_D^{nom}$  for the DCP, COMB<sub>3</sub>DCP, and COMB<sub>6</sub>DCP recoupling sequences. These plots, calculated for a powder of glycine using the same conditions as in Fig. 3, reveal two interesting points. First, it is readily seen that the composite sequences is increasingly robust towards variations in the dipolar coupling relative to the nominal value. This implies that a larger number of the crystallites contribute efficiently to the coherence transfer process, translating directly into improved sensitivity. Also, it is clear that the composite sequences are somewhat more broadbanded with respect to variations in the rf field strengths, and thereby towards rf inhomogeneity. These features explain the conclusions drawn from Fig. 3. The second point to note is that these plots very closely resemble known plots for liquid-state NMR composite inversion pulses [18] where the rf inhomogeneity axis in Fig. 4 is replaced by deviation of the resonance offset relative to the nominal rf field strength (i.e.,  $\Delta\omega/\omega_{rf}^{nom}$ ), while the dipolar coupling deviation is replaced by rf inhomogeneity (i.e.,  $\omega_{rf}/\omega_{rf}^{nom}$ ). This observation reinforces the

very close analogy between composite recoupling sequences and composite liquid-state NMR pulses.

The robustness of the composite recoupling experiments towards non-correlated rf inhomogeneity on the two rf channels and variations in the resonance offsets for the two spin species is analyzed in Fig. 5. It is well-known that the original DCP experiments suffer from relatively little tolerance to both parameters as revealed by the plots in Fig. 5a. Clearly, the COMB<sub>3</sub>DCP and COMB<sub>6</sub>DCP pulse schemes broaden the rf field strength and offset ranges over which efficient dipolar recoupling and thereby coherence transfer may be accomplished. In practical applications the improved robustness towards rf inhomogeneity is particularly important. This applies, for example, in biological solid-state NMR where relative large sample volumes may be required to obtain a reasonable number of spins within the sample volume that besides the relevant molecules should contain membranes, buffers etc to ensure functional conditions. In such cases it is important that all spins contribute to the sensitivity of the experiment independent of their location in the MAS rotor. In practice, it is also desirable to have a relatively broad DCP matching condition. This not only renders the experiment optimization, and the transfer of optimized conditions from sensitive "setup"-samples to less sensitive real samples, much easier but also facilitates preservation of optimal match throughout time-consuming experiments independently on minor variations in the tuning of the rf circuitry. Both aspects become visible in the experimental spectra in Fig. 6 showing the efficiency of  $^{15}\text{N} \rightarrow ^{13}\text{C}$  coherence transfer in  $^{13}\text{C}_\alpha$ - $^{15}\text{N}$ -glycine as function of the field strength on the  $^{13}\text{C}$  rf channel. These spectra quite clearly reveal that the sensitivity of COMB<sub>3</sub>DCP is superior to the DCP experiment and that the rf matching profiles are significantly broader for both compensated experiments as predicted by the theoretical/numerical analysis.

Our results clearly validate the analogy between the simple "Bloch"-picture of rotations in three-dimensional operator coordinate systems, as commonplace for the description of liquid-state NMR composite pulses, and the features of dipolar recoupling. This has been demonstrated on the basis of simple cross-polarization type experiments for heteronuclear coherence transfer with the result of improved compensation of crystallite-induced dispersions in the effective dipolar coupling and improved robustness towards rf inhomogeneity. Both elements contribute to a significant gain in the coherence transfer efficiency and thereby sensitivity of the experiment. From our description it should be clear that the same approach works for both hetero- and homonuclear recoupling experiments. In a simple picture one may consider the original recoupling experiment executed in pieces of different length interrupted by a scaffold of "phase-correcting" hard pulses. Within this

picture, it is straightforward to see that essentially all recoupling experiments may be compensated in the same fashion, with their off-set compensating features maintained or improved. Ideally it should be possible to compensate the experiments to approach 100% coherence transfer for powder samples (i.e., "complete" elimination of the orientation dependency of the coherence transfer) as known from the somewhat longer adiabatic coherence transfer experiments [30, 31]. The optimum length of the recoupling experiment obviously depends on the dipolar scaling factor of the original decoupling experiment, the desired degree of compensation, and effects from relaxation.

## 4 Conclusion

In conclusion, we have demonstrated that analogies between composite rf pulses in liquid-state NMR spectroscopy and common situations for dipolar recoupling in solid-state NMR enables the establishment of general recipes for improving coherence transfer by recoupled dipolar interactions. This improvement is ascribed to the compensation of orientation dependent dispersion of the size of the dipolar coupling induced by variations in the angle  $\beta$  between the internuclear axis and the rotor axis. This compensation, which may be considered a supplement to the popular  $\gamma$ -encoding of many modern dipolar recoupling NMR experiments, leads to substantial improvements of hetero- and homonuclear coherence transfer processes in MAS NMR spectroscopy of powder samples. The principles of the compensated schemes is very general, implying that we foresee that composite recoupling will find widespread applications, for example in biological solid-state NMR spectroscopy.

## References

- [1] S. J. Opella, Nat. Struct. Biol. **4**, 845-848 (1997).
- [2] R. G. Griffin, Nat. Struct. Biol. **5**, 508-512 (1998).
- [3] F. Castellani, B. van Rossum, A. Diehl, M. Schubert, K. Rehbein, and H. Oschkinat, Nature. **420**, 98-102 (2002).
- [4] A. T. Petkova, Y. Ishii, J. J. Balbach, O. N. Antzutkin, R. D. Leapman, F. Deglaglio, and R. Tycko, Proc. Natl. Acad. Sci. **99**, 16742-16747 (2002).
- [5] C. P. Jaroniec, C. E. MacPhee, V.S. Baja, M.T. McMahon, C.M. Dobson, and R. G. Griffin, Proc. Natl. Acad. Sci. **101**, 711-716 (2004).
- [6] J. Schaefer, R. A. McKay and E. O. Stejskal, J. Magn. Reson. **34**, 443-447 (1979).
- [7] T. Gullion and J. Schaefer, J. Magn. Reson. **81**, 196-200 (1989).
- [8] D. P. Raleigh, M. H. Levitt, and R. G. Griffin, Chem. Phys. Lett. **146**, 71-76 (1998).
- [9] N. C. Nielsen, H. Bildsøe, H. J. Jakobsen, and M. H. Levitt, J. Chem. Phys. **101**, 1805-1812 (1994).
- [10] Y. K. Lee, N. D. Kurur, M. Helmle, O.G. Johannessen, N. C. Nielsen, and M. H. Levitt, Chem. Phys. Lett. **242**, 304-309 (1995).
- [11] M. Hohwy, H. J. Jakobsen, M. Eden, M. H. Levitt, and N. C. Nielsen, J. Chem. Phys. **108**, 2686-2694 (1998).
- [12] M. H. Levitt, In *Encyclopedia of NMR* (Wiley, Chichester 2002 ), pp. 165-196.
- [13] U. Haerberlen and J. S. Waugh, Phys. Rev. **175**, 453-467 (1968).
- [14] M. Howhy and N. C. Nielsen, J. Chem. Phys. **109**, 3780-3791 (1998).
- [15] T. Untidt and N. C. Nielsen, Phys. Rev. E. **65**, 021108-1 - 021108-17 (2003).
- [16] M. H. Levitt and R. Freeman, J. Magn. Reson. **43**, 65-80 (1981).
- [17] A. J. Shaka and R. Freeman, J. Magn. Reson. **55**, 487-493 (1983).
- [18] M. H. Levitt, Prog. NMR Spectrosc. **18**, 61-122 (1986).

- [19] L.S. Pontryagin, V. G. Boltyanskii, R. V. Gamkrelidze and E. F. Mishchenko, *The Mathematical Theory of Optimal Processes* (Interscience, New York 1962).
- [20] N. Khaneja, T. Reiss, C. Kehlet, T. Schulte-Herbruggen, and S. J. Glaser, *J. Magn. Reson.* **172**, 296-305 (2005).
- [21] C. T. Kehlet, A. C. Sivertsen, M. Bjerring, T. O. Reiss, N. Khaneja, S. J. Glaser, and N. C. Nielsen, *J. Am. Chem. Soc.* **126**, 10202-10203 (2004).
- [22] C. Kehlet, T. V. Vosegaard, N. Khaneja, S. J. Glaser, and N. C. Nielsen, *Chem. Phys. Lett.* **414**, 204-209 (2005).
- [23] M. Bak, J. T. Rasmussen, and N. C. Nielsen, *J. Magn. Reson.* **147**, 296-330 (2000).
- [24] G.C. Chingas, A.N. Garroway, R.D. Bertrand, and W.B. Moniz, *J. Magn. Reson.* **35**, 283-288 (1979).
- [25] G.C. Chingas, A.N. Garroway, R. D. Bertrand, and W.B. Moniz, *J. Chem. Phys.* **74**, 127-156 (1981).
- [26] S.J. Glaser and J.J. Quant, *Advances in Magnetic and Optical Resonance.* **19**, 59-252 (1996).
- [27] M. Bjerring, J. T. Rasmussen, R. S. Krogshave, and N. C. Nielsen, *J. Chem. Phys.* **119**, 8916-8926 (2003).
- [28] M. Bjerring and N. C. Nielsen, *Chem. Phys. Lett.* **382**, 671-678 (2003).
- [29] K. Kobzar, T.E. Skinner, N. Khaneja, S.J. Glaser, and B. Luy, *J. Magn. Reson.*, **170**, 236-243 (2004).
- [30] M. Baldus, D. G. Geurts, S. Hediger, and B. H. Meier, *J. Magn. Reson. A.* **118**, 140-144 (1996).
- [31] R. Verel, M. Baldus, M. Nijman, J. W. M. Vanus, and B.H. Meier, *Chem. Phys. Lett.* **280**, 31-39 (1997).

## Figure captions

Fig. 1. Trajectories in the  $X^-$ ,  $Y^-$ ,  $Z^-$  subspace for (a) the original DCP experiment (different trajectories correspond to different  $\gamma$  angles (from right  $\gamma=\pi/10$  and equidistant values decreased by  $\pi/10$ ) as well as (b) the  $\beta$ -compensated COMB<sub>3</sub>DCP experiment based on the combination of DCP with composite pulse procedures as described the text. The same trajectories applies to the case of homonuclear double-quantum based coherence transfer experiments by exchanging the  $X^-$ ,  $Y^-$ ,  $Z^-$  axes with  $X^+$ ,  $Y^+$ ,  $Z^+$ .

Fig. 2. Schematic representation of pulse sequences for heteronuclear coherence transfer in MAS solid-state NMR spectroscopy. Double Cross Polarization (DCP) pulse sequences in (a) its conventional form and (b) with with three-element compensation (i.e., COMB<sub>3</sub>DCP). The upper trace represents <sup>1</sup>H irradiation (for <sup>1</sup>H  $\rightarrow$  <sup>15</sup>N coherence transfer and decoupling) applying for both schemes, the different height of the DCP elements (open squares) on <sup>13</sup>C and <sup>15</sup>N reflects mismatch in the rf amplitude by one rotor frequency (e.g.,  $\omega_{rf}^C = \omega_{rf}^N \pm \omega_r$ ) while the number in the elements indicate the length of the element expressed in units of  $\pi/2$  rotations (i.e., in time units of  $\kappa/(2\pi)$ ).

Fig. 3. (a) Efficiencies of <sup>15</sup>N  $\rightarrow$  <sup>13</sup>C coherence transfer calculated for DCP, COMB<sub>3</sub>DCP, and COMB<sub>6</sub>DCP using the parameters of glycine with experimental conditions corresponding to MAS experiments with 10 kHz spinning and using a 700 MHz (Larmor frequency for <sup>1</sup>H) magnet. The various curves reflect homogeneous rf field (solid line), 2% Lorentzian rf inhomogeneity (half width at full height of the rf field distribution around the nominal value; dashed lined), and 5% Lorentzian rf inhomogeneity (dotted line) on both channels using nominal rf field strengths of  $\omega_{rf}/2\pi^C = 35$  kHz and  $\omega_{rf}/2\pi^N = 25$  kHz. (b) Experimental spectra for DCP, COMB<sub>3</sub>DCP, and COMB<sub>6</sub>DCP <sup>15</sup>N  $\rightarrow$  <sup>13</sup>C transfers for a powder of <sup>13</sup>C <sub>$\alpha$</sub> , <sup>15</sup>N-labeled glycine using the same conditions as used for the calculations. The experimental rf inhomogeneity (full 2.5 mm rotor) were estimated to be approximately 5% Lorentzian. The calculations used  $\delta_{aniso}^C = 19.43$  ppm,  $\eta^C = 0.98$ ,  $\{\alpha_{PR}^C, \beta_{PR}^C, \gamma_{PR}^C\} = \{64.9^\circ, 37.3^\circ, -28.8^\circ\}$ ,  $\delta_{aniso}^N = 10.1$  ppm,  $\eta^N = 0.17$ ,  $\{\alpha_{PR}^N, \beta_{PR}^N, \gamma_{PR}^N\} = \{-83.8^\circ, -79.0^\circ, 0.0^\circ\}$ ,  $b_{CN}/2\pi = -890$  Hz,  $\{\alpha_{PR}^{CN}, \beta_{PR}^{CN}, \gamma_{PR}^{CN}\} = \{0^\circ, 0^\circ, 0^\circ\}$ , and  $J_{CN} = -11$  Hz.

Fig. 4. Numerical calculations of the  $^{15}\text{N} \rightarrow ^{13}\text{C}$  coherence transfer for a powder of  $^{13}\text{C}_\alpha, ^{15}\text{N}$ -labeled glycine (10 kHz spinning,  $^1\text{H}$  Larmor frequency of 700 MHz) as function of rf inhomogeneity (expressed as the ratio between the actual rf field strength and the nominal rf field strength, i.e.,  $\omega_{rf}/\omega_{rf}^{nom}$ ) and the deviation in the dipolar coupling expressed as the actual dipolar coupling relative to its nominal values, i.e.,  $\omega_D/\omega_D^{nom}$ ). The nominal rf field strengths were 25 kHz for  $^{15}\text{N}$  and 35 kHz for  $^{13}\text{C}$  (both are varied simultaneously), while the nominal dipolar coupling constant was -890 Hz (parameters as in Fig. 3).

Fig. 5. Rf inhomogeneity (left column) and resonance offset (right column) profiles calculated for (a) DCP, (b) COMB<sub>3</sub>DCP, and (c) COMB<sub>6</sub>DCP for a powder of glycine using the same conditions as in Fig. 3. The color coding used for the contours is identical to this used in Fig. 4.

Fig. 6. Experimental  $^{15}\text{N} \rightarrow ^{13}\text{C}$  coherence transfer efficiencies for  $^{13}\text{C}_\alpha, ^{15}\text{N}$ -labeled glycine (10 kHz spinning,  $^1\text{H}$  Larmor frequency of 700 MHz) recorded as function of the  $^{13}\text{C}$  rf field strength ( $\omega_{rf}^C/2\pi$ ) for DCP (red), COMB<sub>3</sub>DCP (green), and COMB<sub>6</sub>DCP (blue) dipolar recoupling experiments with total excitation times of 1.8, 4.0, and 12.8 ms (ignoring the length of the short phase correcting pulses) and using a  $^{15}\text{N}$  rf field strength of  $\omega_{rf}^N/2\pi = 25$  kHz

Figure 1:

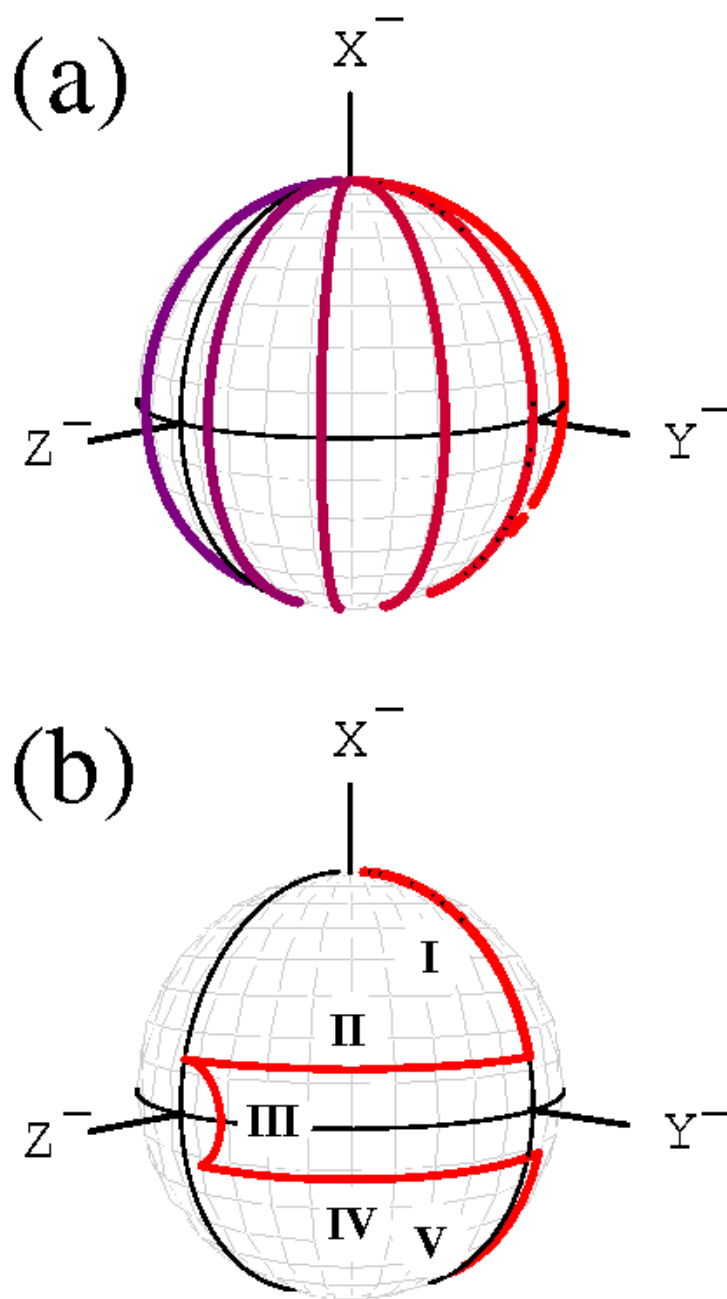


Figure 2:

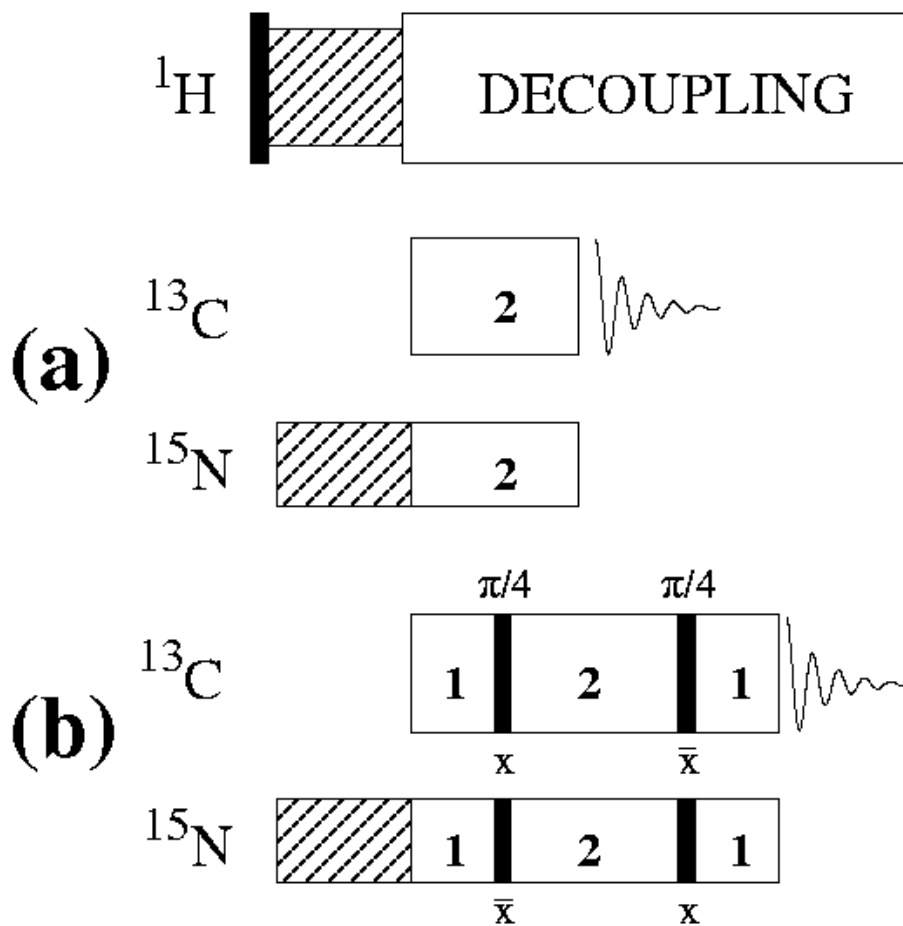


Figure 3:

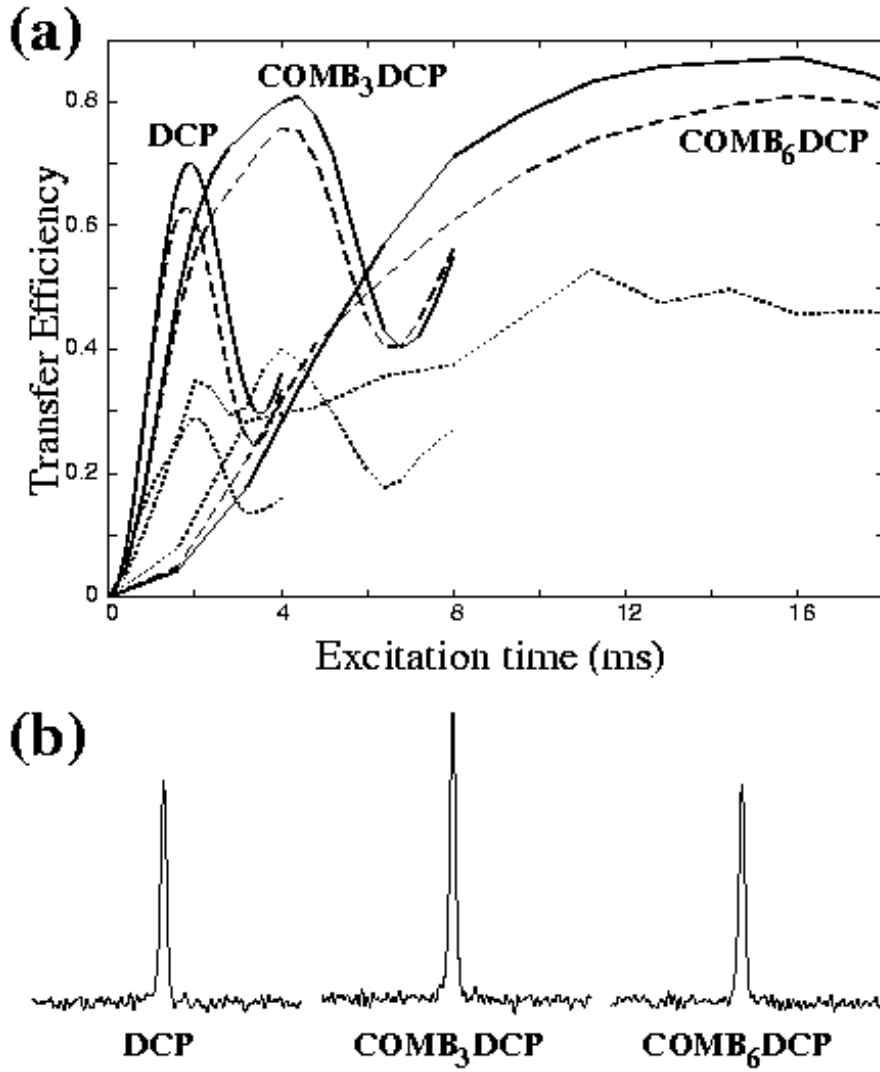


Figure 4:

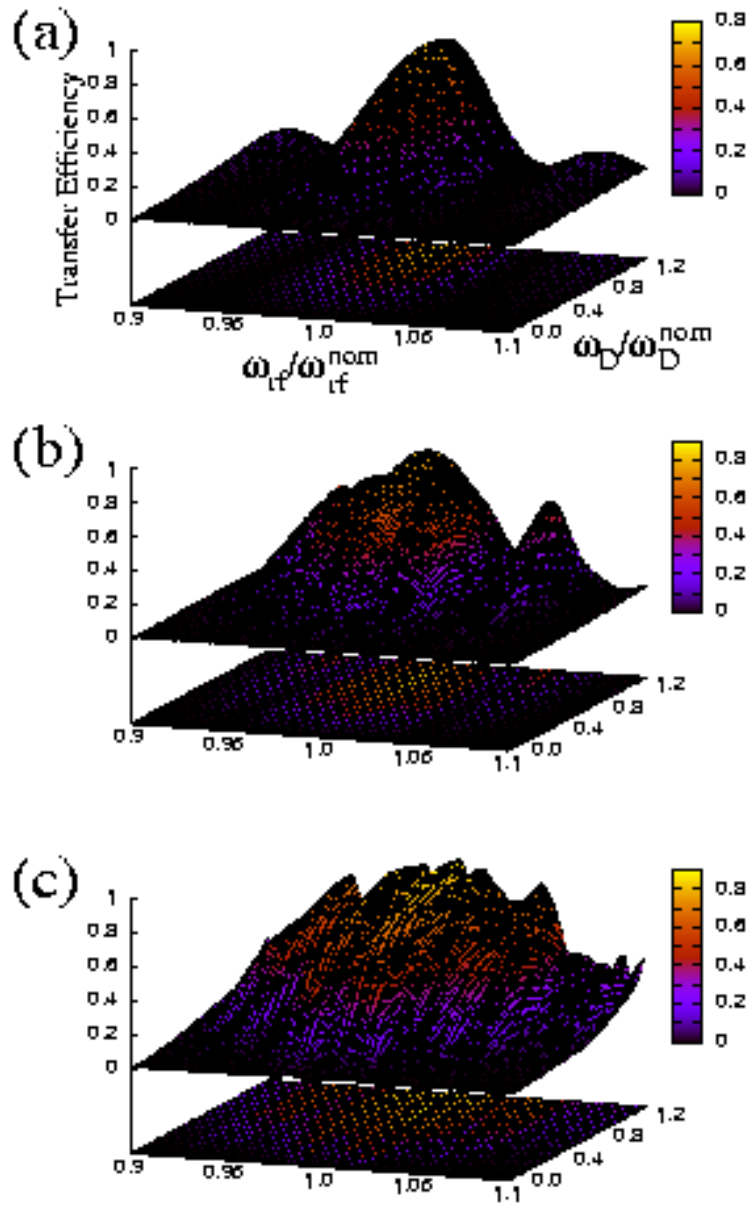


Figure 5:

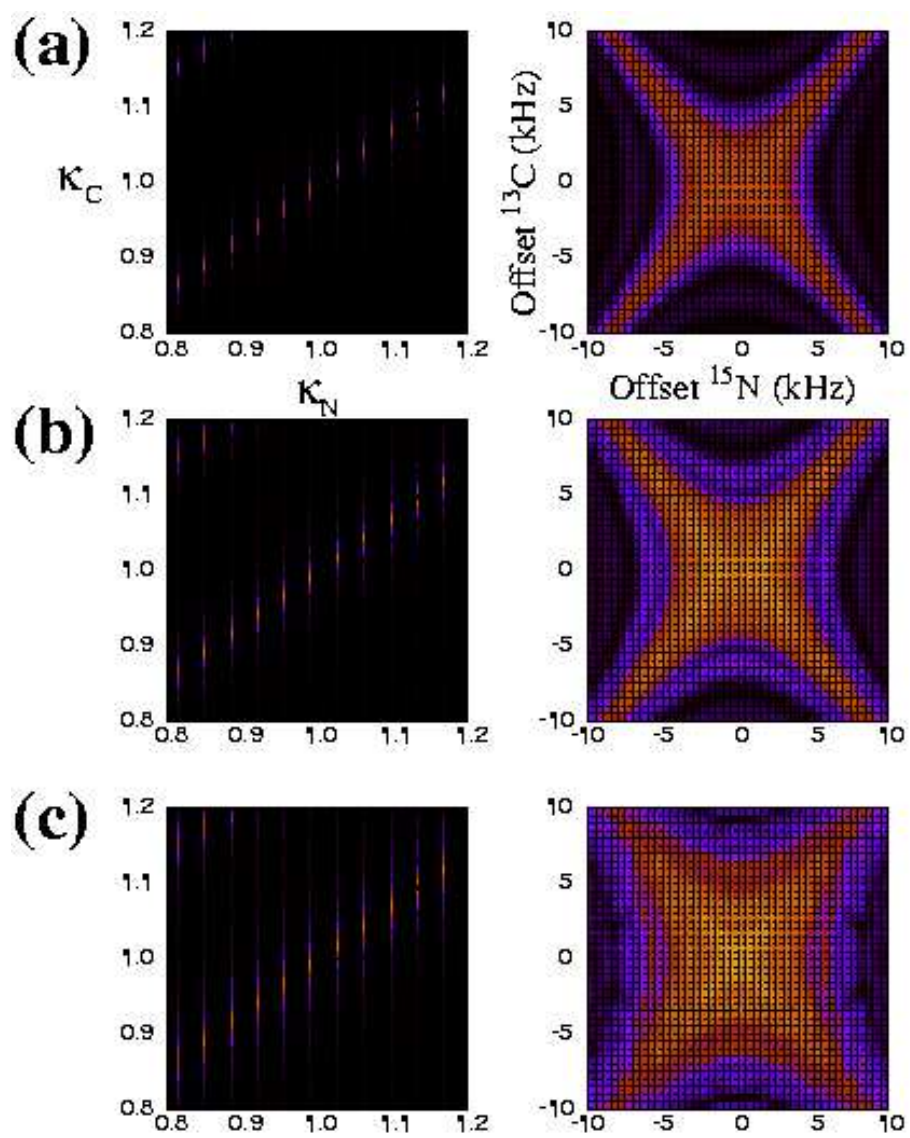


Figure 6:

